Geophys. J. Int. (2008) **175,** 94–102 doi: 10.1111/j.1365-246X.2008.03796.x

On the evaluation of plane-wave reflection coefficients in anelastic media

Rolf Sidler,[1] José M. Carcione[2] and Klaus Holliger[3]

[1] *Institute of Geophysics, ETH Zurich, ETH-Hoenggerberg,* CH-8093 *Zurich, Switzerland*
[2] *Istituto Nazionale di Oceanografia e di Geofisica Sperimentale (OGS), Borgo Grotta Gigante* 42c, I-34010 *Sgonico, Trieste, Italy*
[3] *Institute of Geophysics, University of Lausanne,* CH-1015 *Lausanne, Switzerland. E-mail: klaus.holliger@unil.ch*

Accepted 2008 March 17. Received 2008 February 15; in original form 2007 December 12

SUMMARY

Analytical evaluations of the reflection coefficients in anelastic media inherently suffer from ambiguities related to the complex square roots contained in the expressions of the vertical slowness and polarization. This leads to a large number of mathematically correct but physically unreasonable solutions. To identify the physical solution, we compute full-waveform synthetic seismograms and use a frequency-slowness method for evaluating the amplitude and phase of the corresponding reflection coefficient. We perform this analysis for transversely isotropic media. The analytical solution space and its ambiguities are explored by analysing the paths along the Riemann surfaces associated with the square roots. This analysis allows us to choose the correct sign. Although this approach is generally effective, there are some cases that require an alternative solution, because the correct integration path for the vertical slowness does not exist on the corresponding Riemann surface. Closer inspection then shows that these 'pathological' cases, which are essentially characterized by a higher-attenuation layer overlying a lower-attenuation layer, can readily be resolved through an appropriate change of direction on the Riemann sheet. The thus resulting recipe for the analytical evaluation of plane-wave reflection coefficients in anelastic media is conceptually simple and robust and provides correct solutions beyond the equivalent elastic critical (EEC) angle.

Key words: Elasticity and anelasticity; Seismic anisotropy; Seismic attenuation; Computational seismology; Theoretical seismology.

1 INTRODUCTION

Earth media are generally both attenuating and anisotropic, and hence conventional elastic isotropic approximations prove to be inadequate for fully exploiting the information contained in modern seismic data (Tsvankin & Thomsen 1994; Carcione 2007). It is, in part, for this reason that the problem of effectively evaluating seismic reflection coefficients for layered attenuating media has recently received a significant amount of attention. Although the underlying mathematics is well understood, the problem *per se* must be regarded as unresolved (Nechtschein & Hron 1996; Červený & Pšenčík 2005; Ruud 2006; Krebes & Daley 2007). This is primarily due to the ambiguities related to the signs of the complex-valued square roots involved in the expression of the vertical slownesses, which result in a set of mathematically correct but physically unreasonable plane-wave reflection coefficients.

There are a number of approaches attempting to eliminate these ambiguities. Convergence tests with regard to the well constrained elastic case represent one option. In this case, the reflection coefficient is expected to change smoothly from the purely elastic case to the weakly anelastic case. Although there has been doubt as to the validity of this approach, it is by now widely accepted (Krebes 1984; Richards 1984; Hearn & Krebes 1990). However, Krebes (1984) found that the introduction of little attenuation may lead to substantial phase changes.

Ruud (2006) analysed different criteria to obtain the correct sign of the square roots by comparing seismograms based on analytical reflection coefficients with seismograms computed with a reflectivity algorithm. The presence of a phase difference seems to be related to a particular choice of the anelastic properties for which the amplitudes of reflected/transmitted waves grow exponentially with distance from the interface (Cooper 1967; Richards 1984). The criteria for isotropic media, which are physically relevant but not universally valid, can be summarized as follows.

(1) Impose continuity/smoothness of the reflection coefficient as a function of the incidence angle.

(2) Choose the signs of the square roots according to the direction of the energy-velocity vector: upwards for reflected waves and downwards for transmitted waves.

(3) Apply the radiation condition, meaning that the attenuation vector must point upwards for reflected waves and downwards for transmitted waves, thus implying that the amplitudes of the

waves cannot grow exponentially with increasing distance from the interface.

Ruud (2006) concludes that the energy-velocity vector criterion should be used for pre-critical angles and the radiation condition should be used for post-critical angles, where, in principle, the location of the critical angle is that of the elastic case. He discards the continuity criterion and claims that the coefficients obtained with his approach tend to the elastic coefficients, in particular, the phase angle when the attenuation tends to zero, even if there are discontinuities. In a recent study, Krebes & Daley (2007) compare *SH*-wave reflection coefficients of anelastic media with the elastic equivalent, localize the incidence angles where non-physical jumps or discontinuities occur and explore three different approaches for choosing the sign of the vertical slowness, which they also apply to the *P-SV* case.

The objective of this study is to extend and complement previous work on this problem by providing an effective way to evaluate the reflection coefficients in attenuating anisotropic media. The method consists in the use of full-wave numerical modelling to verify the results and comprehensive rules that allow us to determine the signs of the complex-valued square roots in agreement with the numerical simulations.

We begin with a brief review of the theory for calculating the plane-wave reflection coefficients in attenuating anisotropic media, followed by an overview of the algorithm for the numerical simulation. The modelling algorithm is based on a domain-decomposition technique – one grid for the upper solid and another grid for the lower solid – and the Fourier and Chebyshev differential operators. The anelastic and anisotropic stress–strain relation is based on the Zener model. Special attention is given to modelling the boundary conditions. For this purpose, we further develop the technique for wave propagation in transversely isotropic media. We then present the frequency-slowness approach that allows us to compute the reflection coefficients from the computed seismograms. In the last section, we explore and attempt to resolve the ambiguities present in the analytical solution on the basis of the physically correct solution obtained by numerical modelling.

2 REFLECTION COEFFICIENTS

Without loss of generality, we consider the 2-D *P-SV*-wave case where the relevant elastic constants in the (x, z)-propagation plane are c_{11}, c_{33}, c_{13} and c_{55}. These constants correspond to the unrelaxed, high-frequency limit. We define $c_{11} \equiv \rho v_P^2$ and $c_{55} \equiv \rho v_S^2$, where ρ is the density and v_P and v_S are the *P*- and *S*-wave velocities.

Following Tsvankin (2005), we quantify the degree anisotropy as

$$\epsilon = \frac{c_{11} - c_{33}}{2c_{33}} \tag{1}$$

and the anisotropy parameter $\delta^\star$

$$\delta^\star = \frac{1}{2c_{33}^2}\left[2(c_{13} + c_{44})^2 - (c_{33} - c_{44})(c_{11} + c_{33} - 2c_{44})\right]. \tag{2}$$

Whereas ϵ is related to the fractional difference between the horizontal and vertical *P*-wave velocity, $\delta^\star$ is responsible for the angular dependence of the *P*-wave velocity in the vicinity of the vertical direction, with the *P*-wave velocity increasing away from the vertical if $\delta^\star$ is positive and decreasing if $\delta^\star$ is negative (Tsvankin 2005). The isotropic limit implies $c_{11} = c_{33}$ and $c_{13} = c_{11} - 2c_{55}$ and $\epsilon = \delta^\star = 0$. For the transversely isotropic case, c_{44} is equal to c_{55}.

Given c_{11}, c_{33}, c_{55} and $\delta^\star$, we obtain

$$c_{13} = \sqrt{\frac{2c_{33}^2\delta^\star + (c_{33} - c_{44})(c_{11} + c_{33} + 2c_{44})}{2}} - c_{44}. \tag{3}$$

Therefore, varying $\delta^\star$ means changing c_{13}. In the case of cubic symmetry ($c_{11} = c_{33}$), $\delta^\star$ is the only parameter quantifying the anisotropy. We consider $\epsilon = 0$ in this work.

Reflection and transmission of a wave on a planar interface between two anelastic transversely isotropic media can be estimated using the plane-wave approximation, which has been investigated by several authors, among others Zoeppritz (1919) and Aki & Richards (1980) for isotropic elastic solids, Daley & Hron (1977) and Graebner (1992) for elastic transversely isotropic solids and Carcione (1997) for anelastic transversely isotropic solids. A general plane-wave solution for the particle velocity field is

$$\mathbf{v} = i\omega\mathbf{U}\exp[i\omega(t - s_x x - s_z z)], \tag{4}$$

where t is the time, $i = \sqrt{-1}$ the imaginary unit, ω the angular frequency, s_x and s_z are the horizontal and vertical components of the complex slowness vector, respectively, and

$$\mathbf{U} = U_0\begin{pmatrix}\beta\\ \xi\end{pmatrix}, \tag{5}$$

where U_0 is a constant amplitude.

The polarization components can be calculated as (Carcione 2007)

$$\beta = \sqrt{\frac{p_{55}\,{s_x}^2 + p_{33}\,{s_z}^2 - \rho}{p_{11}\,{s_x}^2 + p_{33}\,{s_z}^2 + p_{55}\left({s_x}^2 + {s_z}^2\right) - 2\rho}} \tag{6}$$

and

$$\xi = \pm\sqrt{\frac{p_{11}\,{s_x}^2 + p_{55}\,{s_z}^2 - \rho}{p_{11}\,{s_x}^2 + p_{33}\,{s_z}^2 + p_{55}\left({s_x}^2 + {s_z}^2\right) - 2\rho}}, \tag{7}$$

where, following the standard sign convention, the '+' sign corresponds to the *qP*-wave and the '−' sign corresponds to the *qS*-wave; moreover, p_{IJ} are components of the stiffness tensor and ρ is the mass density (see Appendix A).

According to Snell's law, the horizontal slowness is the same for all the waves and can be computed for the incident wave as

$$s_x = \frac{\sin\theta}{v_c(\theta)}, \tag{8}$$

where θ is the propagation angle measured with respect to the z-axis and v_c is the complex velocity, solution of the Kelvin–Christoffel equation (Carcione 2007). The vertical slowness can be obtained from the dispersion relation

$$s_z = \pm\frac{1}{\sqrt{2}}\sqrt{K_1 \pm \sqrt{{K_1}^2 - 4K_2K_3}}, \tag{9}$$

where

$$K_1 = \rho\left(\frac{1}{p_{55}} + \frac{1}{p_{33}}\right) + \frac{1}{p_{55}}\left[\frac{p_{13}}{p_{33}}(p_{13} + 2p_{55}) - p_{11}\right]s_x^2,$$

$$K_2 = \frac{1}{p_{33}}\left(p_{11}\,s_x^2 - \rho\right), \qquad K_3 = s_x^2 - \frac{\rho}{p_{55}}.$$

Following the standard sign convention (Carcione 2007), the signs in s_z correspond to

$(+,-)$ downward propagating qP-wave,
$(+,+)$ downward propagating qS-wave,
$(-,-)$ upward propagating qP-wave,
$(-,+)$ upward propagating qS-wave.

For a qP-wave incident from above, the particle velocities above and below the interface are given by

$$\mathbf{v}_1 = \mathbf{v}_{P_I} + \mathbf{v}_{P_R} + \mathbf{v}_{S_R},$$
$$\mathbf{v}_2 = \mathbf{v}_{P_T} + \mathbf{v}_{S_T}, \tag{10}$$

where the subscripts 1 and 2 refer to the upper and lower media and the subscripts I, R and T denote incident, reflected and transmitted plane waves defined as

$$\mathbf{v}_{P_I} = i\omega \begin{pmatrix} \beta_{P_1} \\ \xi_{P_1} \end{pmatrix} \exp[i\omega(t - s_x x - s_{zP_1} z)],$$
$$\mathbf{v}_{P_R} = i\omega R_{PP} \begin{pmatrix} \beta_{P_1} \\ -\xi_{P_1} \end{pmatrix} \exp[i\omega(t - s_x x + s_{zP_1} z)],$$
$$\mathbf{v}_{S_R} = i\omega R_{PS} \begin{pmatrix} \beta_{S_1} \\ -\xi_{S_1} \end{pmatrix} \exp[i\omega(t - s_x x + s_{zS_1} z)],$$
$$\mathbf{v}_{P_T} = i\omega T_{PP} \begin{pmatrix} \beta_{P_2} \\ \xi_{P_2} \end{pmatrix} \exp[i\omega(t - s_x x - s_{zP_2} z)],$$
$$\mathbf{v}_{S_T} = i\omega T_{PS} \begin{pmatrix} \beta_{S_2} \\ \xi_{S_2} \end{pmatrix} \exp[i\omega(t - s_x x - s_{zS_2} z)]. \tag{11}$$

The amplitude of the incident wave U_0 is set to unity so that the amplitudes of the reflected and transmitted waves (R_{PP}, R_{PS}, T_{PP} and T_{PS}) directly correspond to the complex-valued reflection and transmission coefficients.

The boundary conditions on a welded solid-solid interface require continuity of the horizontal and vertical particle velocities v_x and v_z, as well as the components of the stress tensor σ_{xz} and σ_{zz}. The boundary conditions then lead to the following matrix equation for the reflection and transmission coefficients

$$\begin{pmatrix} \beta_{P_1} & \beta_{S_1} & -\beta_{P_2} & -\beta_{S_2} \\ \xi_{P_1} & \xi_{S_1} & \xi_{P_2} & \xi_{S2} \\ Z_{P_1} & Z_{S_1} & -Z_{P_2} & -Z_{S_2} \\ W_{P_1} & W_{S_1} & W_{P_2} & W_{S_2} \end{pmatrix} \begin{pmatrix} R_{PP} \\ R_{PS} \\ T_{PP} \\ T_{PS} \end{pmatrix} = \begin{pmatrix} -\beta_{P_1} \\ \xi_{P_1} \\ -Z_{P_1} \\ W_{P_1} \end{pmatrix}, \tag{12}$$

where

$$W = p_{55}(\xi s_x + \beta s_z) \quad \text{and} \quad Z = \beta p_{13} s_x + \xi p_{33} s_z. \tag{13}$$

In the elastic case, the stiffnesses p_{IJ} correspond to the elastic constants c_{IJ} and have real values. In the viscoelastic case, however, the stiffnesses are complex-valued. It has to be noted that in the anelastic case a critical (and post-critical) angle does not exist (Cooper 1967; Krebes 1983; Carcione 2007) as it refers to the situation where the transmitted wave travels parallel to the interface, which usually does not occur if at least one of the media is anelastic. Therefore, we refer here to the equivalent elastic critical (EEC) angle. The stiffnesses for a transversely isotropic medium are

$$p_{11} = c_{11} - \bar{\mathcal{E}} + \bar{\mathcal{K}} M_1 + c_{55} M_2, \tag{14}$$

$$p_{33} = c_{33} - \bar{\mathcal{E}} + \bar{\mathcal{K}} M_1 + c_{55} M_2, \tag{15}$$

$$p_{13} = c_{13} - \bar{\mathcal{E}} + \bar{\mathcal{K}} M_1 + c_{55}(2 - M_2), \tag{16}$$

and

$$p_{55} = c_{55} M_2, \tag{17}$$

with

$$\bar{\mathcal{E}} = \frac{1}{2}(c_{11} + c_{33}), \quad \bar{\mathcal{K}} = \bar{\mathcal{E}} - c_{55}, \tag{18}$$

and the complex moduli

$$M_\nu = \frac{\sqrt{Q^{(\nu)2} + 1} - 1 + i\,Q^{(\nu)}}{\sqrt{Q^{(\nu)2} + 1} + 1 + i\,Q^{(\nu)}}, \tag{19}$$

where $\nu = 1$ refers to dilatational deformations and $\nu = 2$ to shear deformations and $Q^{(\nu)}$ denotes the corresponding quality factors.

3 NUMERICAL MODELLING

3.1 Governing equations

We consider the stress–strain relation corresponding to the case of two welded transversely isotropic media with the symmetry axis of both media perpendicular to the solid-solid interface. The qP–qSV equations of motion for each medium are given by (1) equations of motion; (2) the stress–strain relations and (3) the memory-variable equations (Carcione 2007), which we outline in the following.

(1) Equations of motion:

$$\partial_x \sigma_{xx} + \partial_z \sigma_{xz} = \rho \partial_t v_x, \tag{20}$$

$$\partial_x \sigma_{xz} + \partial_z \sigma_{zz} = \rho \partial_t v_z. \tag{21}$$

(2) Stress–strain relations:

$$\partial_t \sigma_{xx} = c_{11}\partial_x v_x + c_{13}\partial_z v_z + \bar{\mathcal{K}} e_1 + 2c_{55} e_2 + S, \tag{22}$$

$$\partial_t \sigma_{zz} = c_{13}\partial_x v_x + c_{33}\partial_z v_z + \bar{\mathcal{K}} e_1 - 2c_{55} e_2 + S, \tag{23}$$

$$\partial_t \sigma_{xz} = c_{55}(\partial_z v_x + \partial_x v_z + e_3), \tag{24}$$

where S is the source term corresponding to an isotropic perturbation, such as an explosion, in the upper medium, e_1, e_2 and e_3 are memory variables and

$$\bar{\mathcal{K}} = \bar{\mathcal{E}} - c_{55}, \quad \bar{\mathcal{E}} = \frac{1}{2}(c_{11} + c_{33}). \tag{25}$$

(3) Memory-variable equations:

$$\partial_t e_1 = \frac{1}{\tau_\sigma^{(1)}} \left[\left(\frac{\tau_\sigma^{(1)}}{\tau_\epsilon^{(1)}} - 1 \right) (\partial_x v_x + \partial_z v_z) - e_1 \right], \tag{26}$$

$$\partial_t e_2 = \frac{1}{2\tau_\sigma^{(2)}} \left[\left(\frac{\tau_\sigma^{(2)}}{\tau_\epsilon^{(2)}} - 1 \right) (\partial_x v_x - \partial_z v_z) - 2e_2 \right], \tag{27}$$

$$\partial_t e_3 = \frac{1}{\tau_\sigma^{(2)}} \left[\left(\frac{\tau_\sigma^{(2)}}{\tau_\epsilon^{(2)}} - 1 \right) (\partial_z v_x + \partial_x v_z) - e_3 \right], \tag{28}$$

where $\tau_\sigma^{(\nu)}$ and $\tau_\epsilon^{(\nu)}$ are relaxation times. The frequency-domain stress–strain relations are obtained from the preceding equations by applying the Fourier transform (see Appendix A). The stress–strain relations satisfy the condition that the mean stress depends only on the dilatational relaxation function in any coordinate system, implying that the trace of the stress tensor should

be invariant under coordinate transformations. Moreover, the deviatoric stresses solely depend on the shear relaxation function (Carcione 2007).

3.2 Boundary conditions and modelling algorithm

The boundary conditions at a solid-solid interface require the continuity of the particle velocities v_x and v_z and normal stress components σ_{xz} and σ_{zz}. Two grids model the subdomains above and below the interface. The solution on each grid is obtained by using a Runge–Kutta method for the time stepping and the Fourier and Chebyshev differential operators to compute the spatial derivatives in the horizontal and vertical directions, respectively (Carcione 2007). To combine the two grids, the wavefield is decomposed into incoming and outgoing wave modes at the interface. The inward propagating waves depend on the solution outside the subdomains and therefore are computed from the boundary conditions, whereas the behaviour of the outward propagating waves is determined by the solution inside the subdomain (e.g. Sidler & Carcione 2007). The approach, is adapted here for the anelastic transversely isotropic solid-solid case (axis of symmetry perpendicular to the interface) and involves the equations given in Appendix B for updating the field variables at the gridpoints defining the interface.

3.3 The frequency-slowness method

To compute the numerical reflection coefficient as a function of the incidence angle, we use the technique developed by Kindelan *et al.* (1989) for elastic media and extended by Carcione & Helle (2004) to the case of a viscoelastic seafloor overlain by an acoustic water layer. The method consists on the following steps, where the frequency is denoted by $f = \omega/(2\pi)$:

(1) Generate synthetic seismograms of the pressure field $\sigma_{xx} + \sigma_{zz}$, placing a line of receivers at each gridpoint above the interface. These records contain the incident and reflected fields.

(2) At the same location, compute the synthetic seismogram without interface, by setting the properties of the lower medium to those of the upper medium. These seismograms contain the incident field only.

(3) Take the difference between the wavefields calculated in steps (1) and (2) to isolate the reflected wavefield.

(4) Perform an (f, s_x)-transform of the incident field to obtain $\sigma_I(f, s_x)$.

(5) Perform an (f, s_x)-transform of the reflected field to obtain $\sigma_R(f, s_x)$.

(6) The ratio $|\sigma_R(f, s_x)|/|\sigma_I(f, s_x)|$ corresponds to the absolute value of the reflection coefficient, while its phase angle is given by $\arctan[\sigma_R(f, s_x)/\sigma_I(f, s_x)]$. Transform s_x to incidence angle θ using $\sin\theta = v_{P_1} s_x$, where v_{P_1} is the P-wave velocity of the upper medium.

As we locate the receivers close to the interface, we do not need to correct for the amplitude difference between the incident and the reflected waves.

4 SOLVING THE AMBIGUITIES IN THE EVALUATION OF THE REFLECTION COEFFICIENT

If anelasticity is involved, the analytic expressions for the plane-wave reflection and transmission coefficients contain a number of square roots of complex numbers due to the vertical slownesses (see eq. 9). The square root is the inverse of the square of a function of the form $\sqrt{\lambda^2} = \lambda$. For instance, if $\lambda = -\alpha i$, where α is real, $\sqrt{(-\alpha i)^2}$ can also be written as $\sqrt{(-1)^2(\alpha i)^2}$ so that $\alpha\ i$ as well as $-\ \alpha\ i$ are valid solutions.

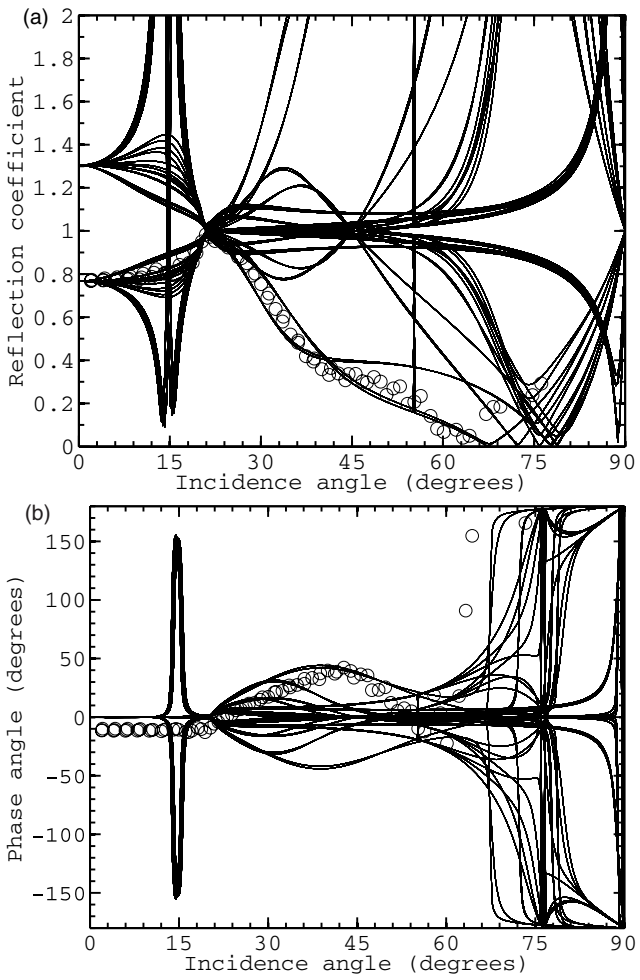

Figure 1. Set of possible solutions for the absolute value (a) and phase angle (b) of the reflection coefficient corresponding to the fluid–solid model given in Table 1 (solid lines). The numerical solution is represented by open circles.

Therefore, the analytical evaluation of reflection coefficients does not result in a unique solution but, due to the nested structure of the complex square root expressions, gives rise to many mathematically correct, but physically unreasonable solutions. Fig. 1, shows the set of all possible solutions for the fluid–solid example given in Table 1. Even if some of these solutions can be discarded based on physical considerations, the remaining subset is still vast. Only one of these solutions corresponds to the physical one. One way of identifying the physical solution is to use numerical modelling. This solution is represented by open circles.

The inherently high computational cost of obtaining numerical solutions does, however, make this approach rather unattractive for many practical applications. One would, therefore, rather find ways to identify the correct signs in the corresponding analytical expressions. The standard sign convention in eqs (7) and (9) is generally valid for incident angles smaller than the EEC angle but may fail for larger angles. This is illustrated in Fig. 2, which compares the analytical solution based on the standard sign convention with the

Table 1. Material properties for the examples.

Fluid-solid case						
Layer	v_P (m s^{-1})	v_S (m s^{-1})	ρ (kg m^{-3})	Q_1	Q_2	$\delta^\star$
1	1500	0.1	1040	10 000	10 000	0
2	4323	1449	2760	40	100	0.1
Solid-solid case						
Layer	v_P (m s^{-1})	v_S (m s^{-1})	ρ (kg m^{-3})	Q_1	Q_2	$\delta^\star$
1	2500	1000	2100	25	15	0
2	5000	3000	2200	40	20	0.1

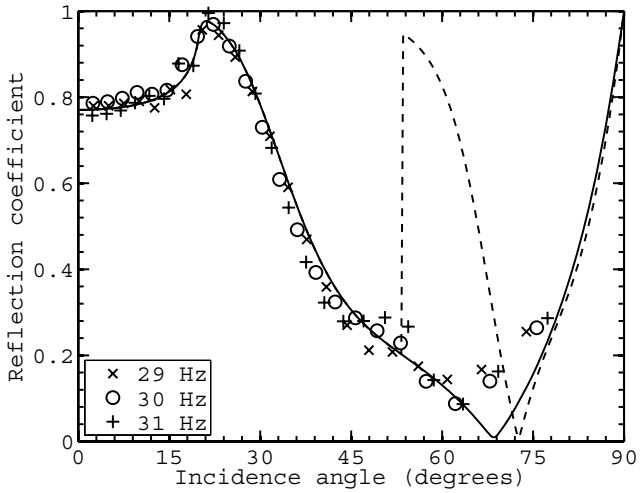

Figure 2. Analytical (dashed and solid lines) and numerical (symbols) solutions for the absolute value of the reflection coefficient for the fluid–solid case given in Table 1. The symbols denote numerical results for different frequencies. The dashed line represents the solution corresponding to the standard sign convention, whereas the solid line corresponds to the solution constrained by enforcing continuity of the vertical slowness by following the Riemann surface of the square root.

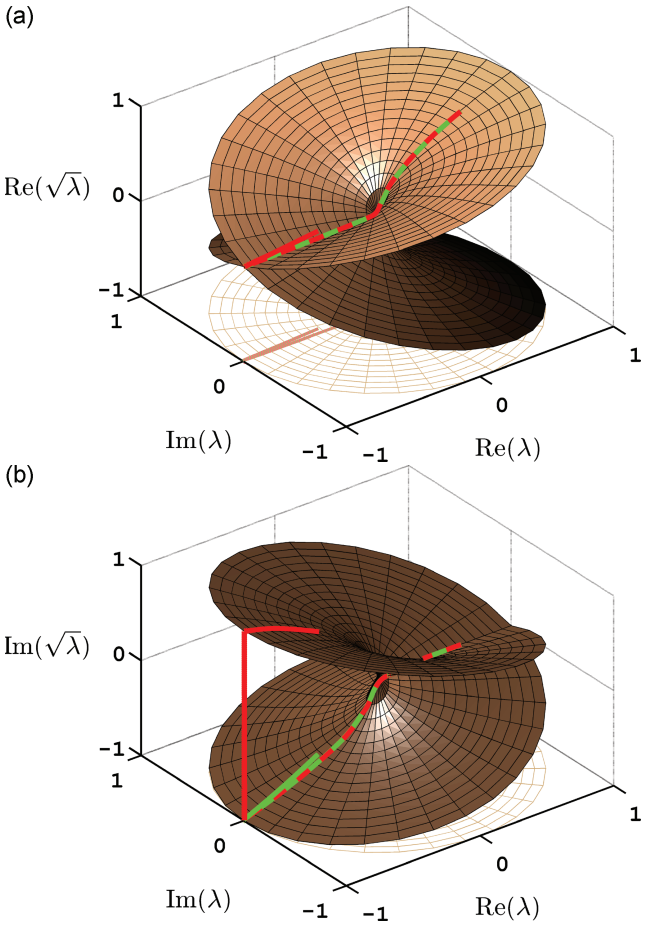

Figure 3. Riemann surface for a complex function of the form $\sqrt{\lambda}$. The 4-D surface is displayed in two 3-D plots, for the real (a) and imaginary (b) parts of the solution. The plots show the path corresponding to square root expressions of the vertical *P*-wave slowness for the fluid-solid case given in Table 1. The red line denotes the path corresponding to the standard sign convention, whereas the green line denotes the path corresponding to the continuous solution following the Riemann surface. The slowness values are normalized for display purposes.

corresponding numerical solution. We see that the two solutions agree well for incidence angles smaller than 53°, whereas for larger angles, the analytical solution is characterized by a seemingly non-physical discontinuity.

In complex analysis, elementary real functions, such as exponentials, square roots, logarithms and trigonometric functions, are expanded into the complex domain and conditions are specified so that the complex functions maintain certain properties of their real-valued counterparts. A particularly common and desirable property of many functions used to describe physical phenomena is their differentiability (Ablowitz & Fokas 2003). To obtain differentiability on an open subset in the complex domain, the so-called Riemann sheets are defined, for which the function is differentiable (Riemann 1857). Such a function is called an analytic function and it can be shown that it is 'infinitely differentiable'. Compared with other complex functions, the complex square root has a relatively simple Riemann surface, which is, however, inherently 4-D in nature and therefore needs two 3-D plots to be visualized (Fig. 3).

Given that the slowness vectors and polarizations of the incident, reflected and transmitted waves are expected to change continuously as a function of the incidence angle, it is reasonable to impose differentiability. This can be achieved by following the Riemann surface when evaluating the corresponding square roots, which assures continuity. In this context, it is important to note that a linear equation system, such as eq. (12), yields continuous results if composed of continuous functions. This in turn ensures that non-physical discontinuities, such as those obtained by using the standard sign convention, can be avoided. Closer inspections shows that the abrupt step in Fig. 2 arises if the square root at an incident angle larger than about 53° is evaluated in the third quadrant of the complex plane, where the standard sign convention indicates the use of the positive sign. Fig. 3 illustrates that this interrupts the continuity of the vertical slowness, as its path does not follow the corresponding Riemann surface. Conversely, we see that the path of the vertical slowness resulting in an analytical solution that is in agreement with the numerical solution, does indeed follow the Riemann surface in a continuous manner.

An additional problem may arise in the calculation of the vertical slowness of the transmitted *P*-wave, if the attenuation of the incident wave is higher than that of the transmitted wave. In such cases, the attenuation vector may point upwards in the vicinity of the EEC angle (Cooper 1967; Richards 1984; Ruud 2006) and the path of the square root expression to calculate the vertical slowness follows the Riemann surface anti-clockwise, implying that in the second quadrant the positive solution has to be chosen. This is at odds with the radiation condition, which postulates the choice of the negative solution for the vertical slowness. For post-critical

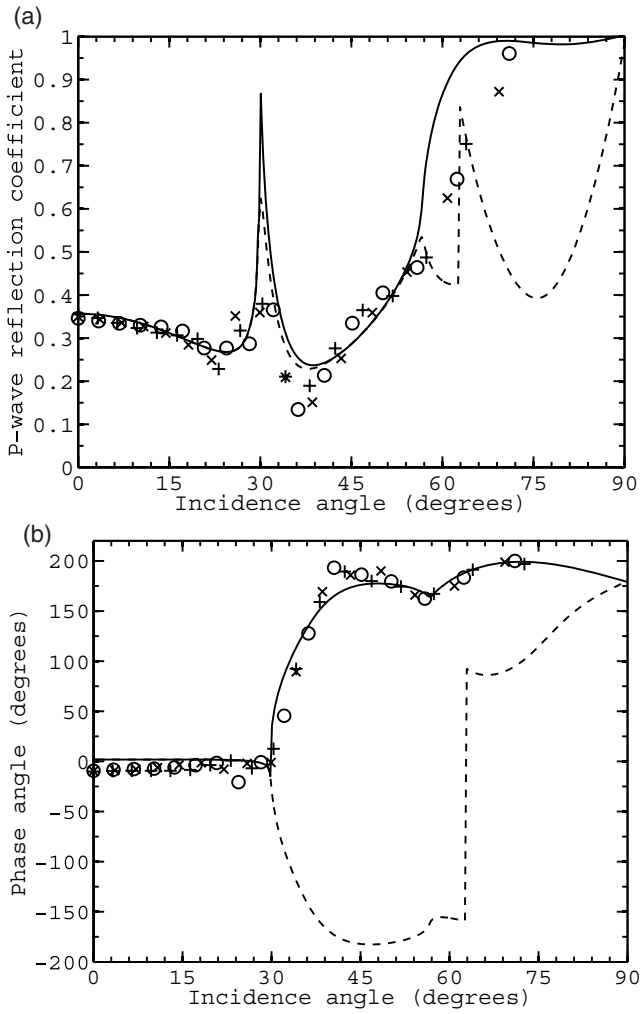

Figure 4. Absolute value (a) and phase angle (b) of the reflection coefficient for the isotropic solid-solid case given in Table 1 ($\delta^\star = 0$). The solution corresponding to the standard sign convention (dashed line) exhibits two problems: abrupt steps in the reflection coefficient due to discontinuous root expressions and a wrong phase due to a 'pathological' behaviour of the attenuation vector. The solid line corresponds to the correct analytical solution and the symbols to numerical solutions for different frequencies ranging between 34 and 36 Hz.

angles of incidence, apart from the immediate vicinity of the EEC angle, the radiation condition is certainly a physically reasonable constraint, which, however, is not honoured by simply ensuring that the path of the vertical slowness follows the Riemann surface. This in turn leads to important phase discrepancies as well as differences in the absolute value of the reflection coefficient compared with the corresponding numerical solution (Figs 4a and b).

Fig. 5 schematically illustrates the difference between a problematic case and an unproblematic case for the calculation of the vertical slowness of the transmitted *P*-wave regarding the behaviour of the argument of the square root. The difference resides in the location of the intersection between the argument and the real axis. If this intersection is located on the negative real axis, we have an unproblematic case. Conversely, if this intersection is located in the positive real axis, we have a problematic case and simply following the Riemann surface leads to substantial errors at large incidence angles. A possible way to address and alleviate this problem is to choose the negative solution for the vertical slowness in the second

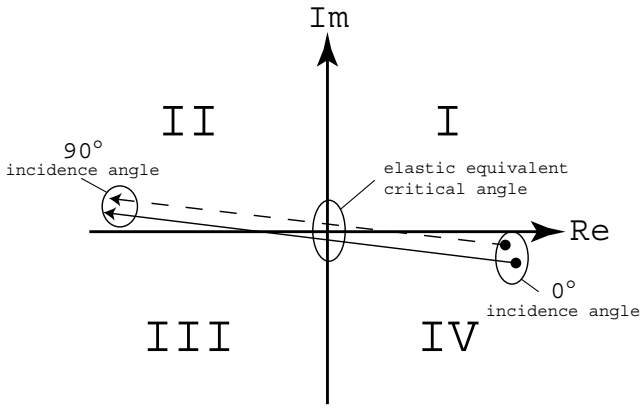

Figure 5. Complex-valued argument of the square root to calculate the vertical slowness of the transmitted *P*-wave. It is shown how to distinguish a problematic case (dashed line) from an unproblematic (solid line) case by following the Riemann surface to obtain physically meaningful results. In the unproblematic case, where the Riemann surface has to be followed, the argument intersects the negative real axis. Conversely, in the problematic case, the intersection occurs along the positive real axis. In this case, continuous solutions follow the positive Riemann sheet after the EEC angle (see Fig. 3). On this Riemann sheet, the imaginary part is positive, thus corresponding to a reversed attenuation vector, which is, however, not likely to be the case outside the immediate vicinity of the EEC angle. Here, the Riemann surface should not be followed and the negative solution in the second quadrant should be chosen.

quadrant of the complex plane irrespective of the path of the square root expressions in the Riemann surface. This approach is admittedly pragmatic and heuristic, but also highly effective for practical purposes and rather general in nature. As illustrated in Fig. 4, it generates a solution that is consistent with the numerical one.

The isotropic solid-solid model corresponding to Fig. 4 (Table 1) is taken from Krebes & Daley (2007). This example is of particular interest as it suffers from both problems discussed in this paper. The absolute value of the reflection coefficient and its phase exhibit considerable discontinuities at an incident angle of approximately 63°, which can be avoided by evaluating the root expressions following the Riemann surface. Doing so, does, however, still result in a phase angle that is entirely inconsistent with that inferred by numerical modelling at angles larger than the EEC angle of about 30°. This is due to the fact that the attenuation is higher in the incident medium, and therefore the argument of the square root corresponding to the transmitted *P*-wave intersects the positive real axis, which makes this case one of the exceptions discussed before.

Fig. 6 shows the path of the square root expressions of the vertical slowness of the transmitted *S*-wave corresponding to the isotropic solid-solid case. This slowness suffers from discontinuities when the standard sign convention is used and the Riemann-surface criterion is not followed. The discontinuity is also visible at an incidence angle of approximately 63° in the corresponding absolute value of the reflection coefficient, and it is even more pronounced in the phase angle (Fig. 4). Fig. 7, addressing the problematic case, shows the path of the square root expression of the vertical slowness of the transmitted *P*-wave. The red line corresponds to the path following the Riemann surface, whereas the green line shows the choice of the negative solution in the second quadrant. The latter solution corresponds to the heuristic approach proposed above and leads to a result that is not entirely correct in the vicinity of the EEC angle, but it is otherwise consistent with the numerical solution.

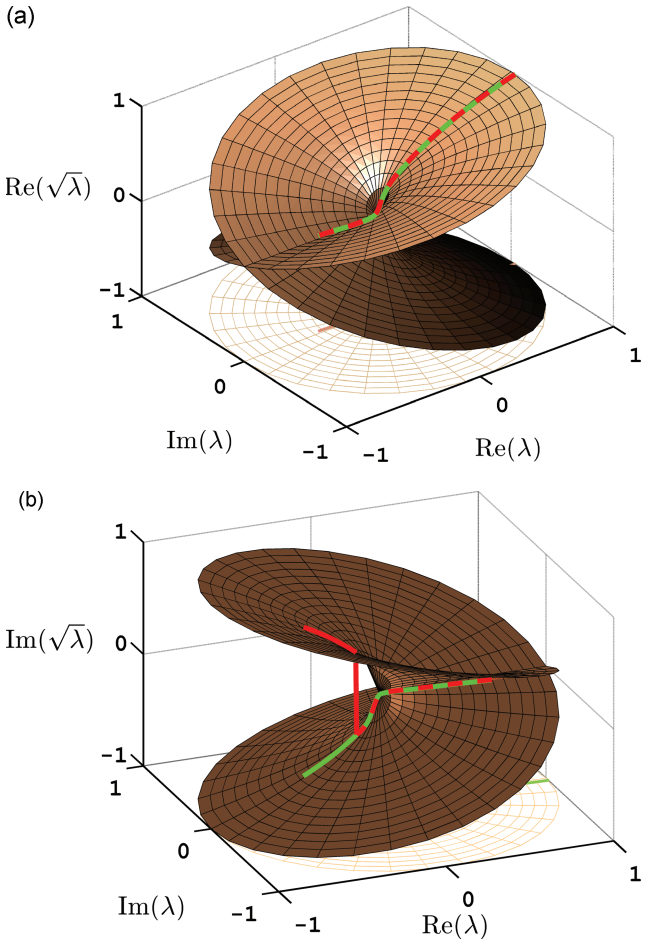

Figure 6. Real (a) and imaginary (b) parts of the square root involved in the vertical *S*-wave slowness of the lower half-space for the isotropic solid-solid case given in Table 1 ($\delta^\star = 0$). The green line corresponds to the continuous solution obtained by following the Riemann surface and the red line to the solution resulting from the standard sign convention. Note the abrupt step in the path corresponding to the standard convention, which is also present in the reflection coefficient and phase angle shown in Fig. 4. The slowness values are normalized for display purposes.

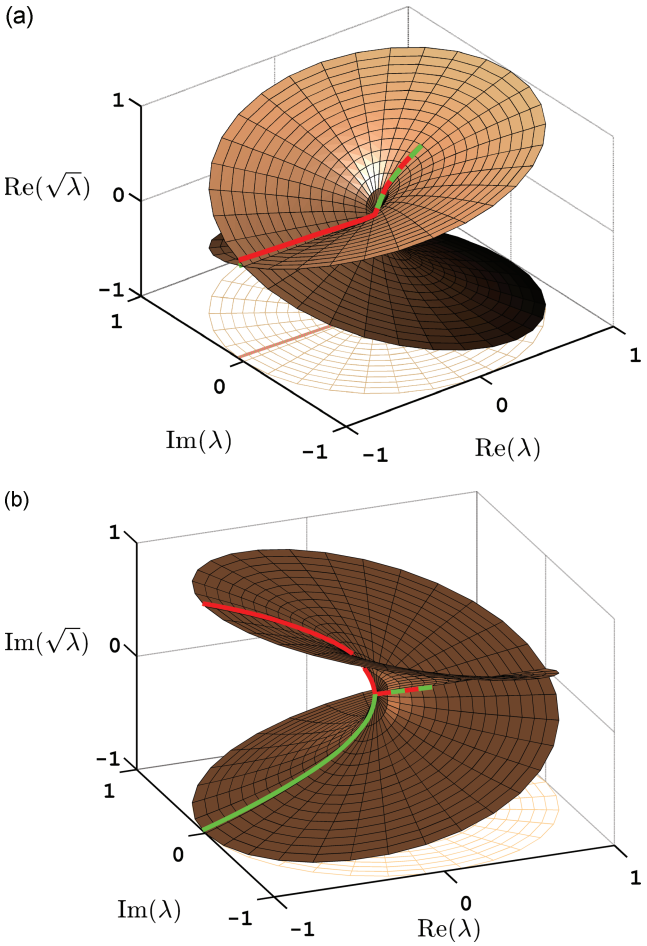

Figure 7. Real (a) and imaginary (b) parts of the square root involved in the vertical *P*-wave slowness of the lower half-space for the isotropic solid-solid case given in Table 1. The red line corresponds to a continuous sign choice, which is problematic in this case (see also Figs 4 and 5) and leads to a wrong phase angle beyond the EEC angle. A simple but effective solution is to choose the negative sign for the square root expression of vertical *P*-wave slowness of the lower solid in the second quadrant (green line). The slowness values are normalized for display purposes.

The last example has the same parameters as the first solid-solid case, albeit with anisotropy added (Table 1). It is interesting and important to note that this rather minor amount of anisotropy leads to additional and rather dramatic complications with regard to the previously considered isotropic case (Fig. 4). The result obtained by using the standard sign convention again yields seemingly non-physical effects beyond the EEC angle, whereas following the Riemann-surface criterion and choosing the negative solution for the vertical slowness of the transmitted *P*-wave, as indicated in Fig. 5, leads to reasonable changes compared with the isotropic case and an analytical solution that is consistent with its numerical counterpart (Fig. 8).

It is important to note that this approach is essentially an alternative formulation of the recipe proposed by Krebes & Daley (2007), which is based on the enforcement of continuity of the vertical slowness in the pre-critical range and honouring the radiation condition in the post-critical range. While the two ways of arriving at this solution are evidently equivalent, and the formulation by Krebes & Daley (2007) favours physical intuition, we believe that our approach will prove to be quite suitable from an algorithmic point of view.

5 CONCLUSIONS

We have used an accurate numerical technique, based on a frequency-slowness approach, to evaluate plane-wave reflection coefficients in anelastic anisotropic layered media to systematically explore the inherent ambiguities associated with the corresponding analytical solutions. Our results indicate that the continuity criterion based on continuous paths along the Riemann surfaces of the square root expressions associated with the complex slownesses provides a convenient solution to resolve the ambiguities in the calculation of the reflection coefficients. However, there exist some cases for which a continuous path does not exist on the corresponding Riemann surface. These cases can be identified by the intersection of the argument of the square root with the positive real axis. Our results demonstrate that in these problematic, but well defined, cases an appropriate change of direction on the Riemann surface provides physically correct solutions for all practical applications beyond the vicinity of the EEC angle. The approach developed here is essentially equivalent to enforcing continuity of the vertical slowness in the pre-critical range and honouring the radiation condition in the post-critical range.

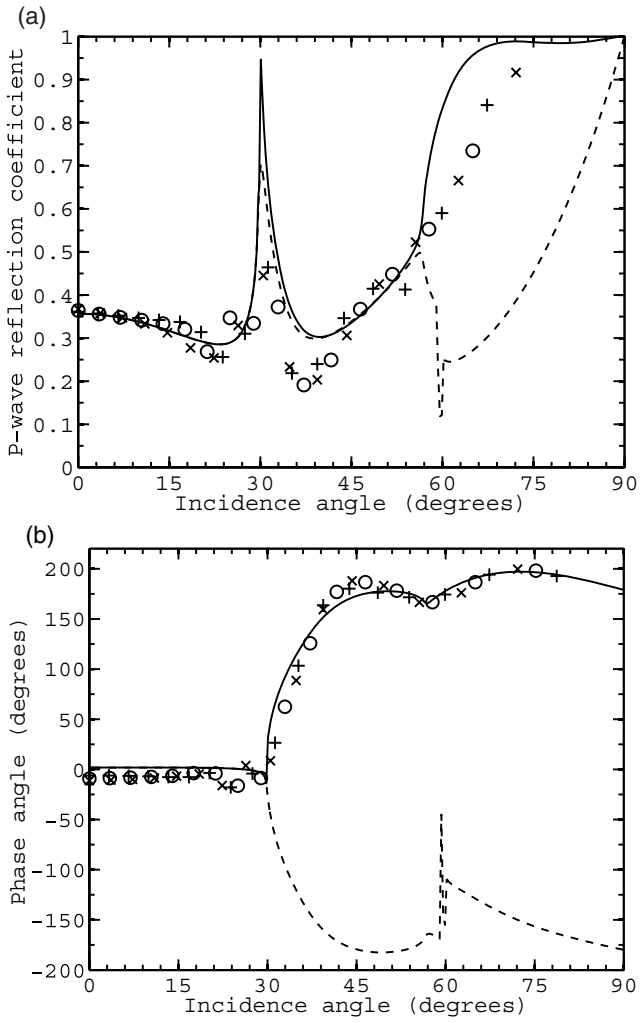

Figure 8. Absolute value (a) and phase angle (b) of the reflection coefficient for the anisotropic solid-solid case given in Table 1. The solid line corresponds to the physically correct solution whereas the dashed line is the solution obtained when choosing the standard sign convention for all the square roots. The symbols denote numerical solutions for frequencies ranging between 34 and 36 Hz. Note that even though the amount of anisotropy present is rather weak, the solution using the standard sign convention (dashed line) shows large differences compared with the corresponding isotropic solution shown in Fig. 4.

ACKNOWLEDGMENTS

The authors thank Stewart Greenhalgh, editor Johan Robertsson and two anonymous reviewers for their constructive comments and suggestions that improved the paper. This project was funded by the European Commission's Human Resources and Mobility Program, Marie Curie Research Training Network SPICE Contract MRTN-CT-2003-504267.

REFERENCES

Ablowitz, M.J. & Fokas, A.S., 2003. *Complex Variables*, 2nd edn, Cambridge University Press, Cambridge.

Aki, K. & Richards, P.G., 1980. *Quantitative Seismology*, Freeman, San Francisco.

Carcione, J.M., 1997. Reflection and transmission of qP-qS plane waves at a plane boundary between viscoelastic transversely isotropic media, *Geophys. J. Int.,* **129,** 669–680.

Carcione, J.M., 2007. *Wave Fields in Real Media: Wave Propagation in Anisotropic, Anelastic, Porous and Electromagnetic media,* 2nd edn, Elsevier Science, Amsterdam.

Carcione, J.M. & Helle, H.B., 2004. On the physics and simulation of wave propagation at the ocean bottom: *Geophysics,* **69,** 825–839.

Carcione, J.M., Herman, G. & ten Kroode, A.P.E., 2002. Seismic modeling, *Geophysics,* **67,** 1304–1325.

Červený, V. & Pšenčík, I., 2005. Plane waves in viscoelastic anisotropic media – I. Theory, *Geophys. J. Int.,* **161,** 197–212.

Cooper, H.F., 1967. Reflection and transmission of oblique plane waves at a plane interface between viscoelastic media, *J. acoust. Soc. Am.,* **42,** 1064–1069.

Daley, P.F. & Hron, F., 1977. Reflection and transmission coefficients for transversely isotropic media, *Bull. seism. Soc. Am.,* **67,** 661–675.

Graebner, M., 1992. Plane-wave reflection and transmission coefficients for a transversely isotropic solid, *Geophysics,* **57,** 1512–1519.

Hearn, D.J. & Krebes, E.S., 1990. On computing ray-synthetic seismograms for anelastic media using complex rays, *Geophysics,* **55,** 422–432.

Kindelan, M., Seriani, G. & Sguazzero, P., 1989. Elastic modeling and its application to amplitude versus angle interpretation, *Geophys. Prospect.,* **37,** 3–30.

Krebes, E.S., 1983. The viscoelastic reflection/transmission problem: two special cases, *Bull. seism. Soc. Am.,* **73,** 1673–1683.

Krebes, E.S., 1984. On the reflection and transmission of viscoelastic waves – some numerical results, *Geophysics,* **49,** 1374–1380.

Krebes, E.S. & Daley, P.F., 2007. Difficulties with computing anelastic plane-wave reflection and transmission coefficients, *Geophys. J. Int.,* **170,** 205–216.

Nechtschein, S. & Hron, F., 1996. Reflection and transmission coefficients between two anelastic media using asymptotic ray theory, *Can. J. Explor. Geophys.,* **32,** 31–40.

Richards, P.G., 1984. On wave fronts and interfaces in anelastic media, *Bull. seism. Soc. Am.,* **74,** 2157–2165.

Riemann, B., 1857. Theorie der Abel'schen Functionen, *Journal für die reine und angewandte Mathematik,* **54,** 101–155.

Ruud, B.O., 2006. Ambiguous reflection coefficients for anelastic media, *Stud. Geophys. Geod.,* **50,** 479–498.

Sidler, R. & Carcione, J.M., 2007. Wave reflection at an anelastic anisotropic ocean bottom, *Geophysics,* **72,** SM139–SM146.

Tessmer, E., Kessler, D., Kosloff, D. & Behle, A., 1992. Multi-domain Chebyshev-Fourier method for the solution of the equations of motion of dynamic elasticity, *J. Comput. Phys.,* **100,** 355–363.

Tsvankin, I., 2005. *Seismic Signatures and Analysis of Reflection Data in Anisotropic Media,* 2nd edn, Elsevier Science, Amsterdam.

Tsvankin, I. & Thomsen, L., 1994. Nonhyperbolic reflection moveout in anisotropic media, *Geophysics,* **59,** 1290–1304.

Zener, C., 1948. *Elasticity and Anelasticity of Metals,* University of Chicago Press, Chicago.

Zoeppritz, K., 1919. Über Erdbebenwellen VII B: Über Reflexion und Durchgang seismischer Wellen durch Unstetigkeitsflächen: *Göttinger Nachrichten,* **1,** 66–84.

APPENDIX A: FREQUENCY-DOMAIN STRESS–STRAIN RELATION

Transforming the memory-variable eqs (26)–(28) to the (frequency) ω-domain (e.g. $\partial_t e_1 \rightarrow i\omega e_1$) and substituting the memory variables into eqs (22)–(24), we obtain the stress–strain relation:

$$i\omega \begin{pmatrix} \sigma_{xx} \\ \sigma_{zz} \\ \sigma_{xz} \end{pmatrix} = \begin{pmatrix} p_{11} & p_{13} & 0 \\ p_{13} & p_{33} & 0 \\ 0 & 0 & p_{55} \end{pmatrix} \begin{pmatrix} \partial_x v_x \\ \partial_z v_z \\ \partial_z v_x + \partial_x v_x \end{pmatrix}, \qquad \text{(A1)}$$

where

$$
\begin{aligned}
p_{11} &= c_{11} - \bar{\mathcal{E}} + \bar{\mathcal{K}} M_1 + c_{55} M_2, \\
p_{33} &= c_{33} - \bar{\mathcal{E}} + \bar{\mathcal{K}} M_1 + c_{55} M_2, \\
p_{13} &= c_{13} - \bar{\mathcal{E}} + \bar{\mathcal{K}} M_1 + c_{55}(2 - M_2), \\
p_{55} &= c_{55} M_2
\end{aligned}
\tag{A2}
$$

are the complex stiffnesses, and

$$
M_\nu = \frac{\tau_\sigma^{(\nu)}}{\tau_\epsilon^{(\nu)}} \left(\frac{1 + i\omega\tau_\epsilon^{(\nu)}}{1 + i\omega\tau_\sigma^{(\nu)}} \right), \quad \nu = 1, 2 \tag{A3}
$$

are the Zener complex moduli (Zener 1948; Carcione 2007). Note that for $\omega \to \infty$ we have $p_{IJ} \to c_{IJ}$.

The relaxation times can be expressed as

$$
\tau_\epsilon^{(\nu)} = \frac{\tau_0}{Q_\nu} \left(\sqrt{Q_\nu^2 + 1} + 1 \right) \quad \text{and} \quad \tau_\sigma^{(\nu)} = \frac{\tau_0}{Q_\nu} \left(\sqrt{Q_\nu^2 + 1} - 1 \right), \tag{A4}
$$

where τ_0 is a relaxation time such that $1/\tau_0$ is the centre frequency of the relaxation peak and Q_ν are the minimum quality factors.

APPENDIX B: BOUNDARY EQUATIONS

The upper solid is denoted by the subscript 1 and the lower solid by the subscript 2. The symbol P indicates the compressional wave in the fluid or the qP-wave in solid, and S denotes the qS-wave in this medium. The boundary equations at the solid–solid interface for the transversely isotropic case (the interface perpendicular to the symmetry axis) are generalizations of the equations given in Tessmer *et al.* (1992) for the isotropic case:

$$
\begin{aligned}
v_x^{(\mathrm{new})}(1) &= [Z_S(1) + Z_S(2)]^{-1} \Big[Z_S(2) v_x^{(\mathrm{old})}(2) + Z_S(1) v_x^{(\mathrm{old})}(1) \\
&\quad + \sigma_{xz}^{(\mathrm{old})}(1) - \sigma_{xz}^{(\mathrm{old})}(2) \Big], \\
v_z^{(\mathrm{new})}(1) &= [Z_P(1) + Z_P(2)]^{-1} \Big[Z_P(2) v_z^{(\mathrm{old})}(2) + Z_P(1) v_z^{(\mathrm{old})}(1) \\
&\quad + \sigma_{zz}^{(\mathrm{old})}(1) - \sigma_{zz}^{(\mathrm{old})}(2) \Big], \\
\sigma_{xx}^{(\mathrm{new})}(1) &= \sigma_{xx}^{(\mathrm{old})}(1) + \Big[c_{13}(1)/c_{33}(1) \Big] \Big[\sigma_{zz}^{(\mathrm{new})}(1) - \sigma_{zz}^{(\mathrm{old})}(1) \Big], \\
\sigma_{xz}^{(\mathrm{new})}(1) &= \frac{Z_S(1) Z_S(2)}{Z_S(1) + Z_S(2)} \left[v_x^{(\mathrm{old})}(1) - v_x^{(\mathrm{old})}(2) + \frac{\sigma_{xz}^{(\mathrm{old})}(1)}{Z_S(1)} \right. \\
&\quad \left. + \frac{\sigma_{xz}^{(\mathrm{old})}(2)}{Z_S(2)} \right], \\
\sigma_{zz}^{(\mathrm{new})}(1) &= \frac{Z_P(1) Z_P(2)}{Z_P(1) + Z_P(2)} \left[v_z^{(\mathrm{old})}(1) - v_z^{(\mathrm{old})}(2) + \frac{\sigma_{zz}^{(\mathrm{old})}(1)}{Z_P(1)} \right. \\
&\quad \left. + \frac{\sigma_{zz}^{(\mathrm{old})}(2)}{Z_P(2)} \right],
\end{aligned}
$$

$$
\begin{aligned}
e_1^{(\mathrm{new})}(1) &= e_1^{(\mathrm{old})}(1) + [\phi_1(1)/c_{33}(1)] \Big[\sigma_{zz}^{(\mathrm{new})}(1) - \sigma_{zz}^{(\mathrm{old})}(1) \Big] \\
e_2^{(\mathrm{new})}(1) &= e_2^{(\mathrm{old})}(1) - [\phi_2(1)/c_{33}(1)] \Big[\sigma_{zz}^{(\mathrm{new})}(1) - \sigma_{zz}^{(\mathrm{old})}(1) \Big], \\
e_3^{(\mathrm{new})}(1) &= e_3^{(\mathrm{old})}(1) + [\phi_2(1)/c_{55}(1)] \Big[\sigma_{xz}^{(\mathrm{new})}(1) - \sigma_{xz}^{(\mathrm{old})}(1) \Big], \\
v_x^{(\mathrm{new})}(2) &= v_x^{(\mathrm{new})}(1), \\
v_z^{(\mathrm{new})}(2) &= v_z^{(\mathrm{new})}(1), \\
\sigma_{xx}^{(\mathrm{new})}(2) &= \sigma_{xx}^{(\mathrm{old})}(2) + [c_{13}(2)/c_{33}(2)] \Big[\sigma_{zz}^{(\mathrm{new})}(2) - \sigma_{zz}^{(\mathrm{old})}(2) \Big], \\
\sigma_{xz}^{(\mathrm{new})}(2) &= \sigma_{xz}^{(\mathrm{new})}(1), \\
\sigma_{zz}^{(\mathrm{new})}(2) &= \sigma_{zz}^{(\mathrm{new})}(1), \\
e_1^{(\mathrm{new})}(2) &= e_1^{(\mathrm{old})}(2) + [\phi_1(2)/c_{33}(2)] \Big[\sigma_{zz}^{(\mathrm{new})}(2) - \sigma_{zz}^{(\mathrm{old})}(2) \Big], \\
e_2^{(\mathrm{new})}(2) &= e_2^{(\mathrm{old})}(2) - [\phi_2(2)/c_{33}(2)] \Big[\sigma_{zz}^{(\mathrm{new})}(2) - \sigma_{zz}^{(\mathrm{old})}(2) \Big], \\
e_3^{(\mathrm{new})}(2) &= e_3^{(\mathrm{old})}(2) + [\phi_2(2)/c_{55}(2)] \Big[\sigma_{xz}^{(\mathrm{new})}(2) - \sigma_{xz}^{(\mathrm{old})}(2) \Big],
\end{aligned}
\tag{B1}
$$

where $\phi_\nu = 1/\tau_\epsilon^{(\nu)} - 1/\tau_\sigma^{(\nu)}$, $Z_P = \sqrt{\rho c_{33}}$ and $Z_S = \sqrt{\rho c_{55}}$.

The lower boundary of subdomain 2 (lower medium) satisfies the non-reflecting conditions

$$
\begin{aligned}
v_x^{(\mathrm{new})} &= \frac{1}{2} \Big(v_x^{(\mathrm{old})} + \sigma_{xz}^{(\mathrm{old})}/Z_S \Big), \\
v_z^{(\mathrm{new})} &= \frac{1}{2} \Big(v_z^{(\mathrm{old})} + \sigma_{zz}^{(\mathrm{old})}/Z_P \Big), \\
\sigma_{xx}^{(\mathrm{new})} &= \sigma_{xx}^{(\mathrm{old})} - (c_{13}/2c_{33}) \Big(\sigma_{zz}^{(\mathrm{old})} - Z_P v_z^{(\mathrm{old})} \Big), \\
\sigma_{zz}^{(\mathrm{new})} &= \frac{1}{2} \Big(\sigma_{zz}^{(\mathrm{old})} + Z_P v_z^{(\mathrm{old})} \Big), \\
\sigma_{xz}^{(\mathrm{new})} &= \frac{1}{2} \Big(\sigma_{xz}^{(\mathrm{old})} + Z_S v_x^{(\mathrm{old})} \Big), \\
e_1^{(\mathrm{new})} &= e_1^{(\mathrm{old})} - [\phi_1/(2c_{33})] \Big(\sigma_{zz}^{(\mathrm{old})} - Z_P v_z^{(\mathrm{old})} \Big), \\
e_2^{(\mathrm{new})} &= e_2^{(\mathrm{old})} + [\phi_2/(2c_{33})] \Big(\sigma_{zz}^{(\mathrm{old})} - Z_P v_z^{(\mathrm{old})} \Big), \\
e_3^{(\mathrm{new})} &= e_3^{(\mathrm{old})} - [\phi_2/(2c_{55})] \Big(\sigma_{xz}^{(\mathrm{old})} - Z_S v_x^{(\mathrm{old})} \Big),
\end{aligned}
\tag{B2}
$$

where the index 2 has been omitted for brevity. The upper boundary of the upper medium also satisfies non-reflecting conditions. To obtain the equations for this boundary, the method requires the following substitutions: $z \to -z$, which implies $v_z \to -v_z$, $\sigma_{xz} \to -\sigma_{xz}$ and $e_3 \to -e_3$.

In addition to the non-reflecting conditions, absorbing strips are used to further attenuate the wavefield at non-physical boundaries (Carcione *et al.* 2002).